Full-Scale Crash Tests and Analyses of Three High-Wing Single Engine Aircraft

Martin S. Annett

Structural Dynamics Branch

NASA Langley Research Center

Hampton, VA, USA

Justin D. Littell

Structural Dynamics Branch

NASA Langley Research Center

Hampton, VA, USA

Chad M. Stimson

Structural and Thermal Systems Branch

NASA Langley Research Center

Hampton, VA, USA

Karen E. Jackson

Structural Dynamics Branch

NASA Langley Research Center

Hampton, VA, USA

Brian H. Mason

Durability, Damage Tolerance, & Reliability Branch

NASA Langley Research Center

Hampton, VA, USA

Full-Scale Crash Tests and Analyses of Three High-Wing Single Engine Aircraft

The NASA Emergency Locator Transmitter Survivability and Reliability (ELTSAR) project was initiated in 2013 to assess the crash performance standards for the next generation of emergency locator transmitter (ELT) systems. Three Cessna-172 aircraft were acquired to conduct crash testing at NASA Langley Research Center's Landing and Impact Research Facility. Testing was conducted in the summer of 2015 that represented three crash conditions; a flare to stall during emergency landing, and two controlled flight into terrain scenarios. Instrumentation and video coverage, both onboard and external, provided valuable data of airframe response. Full-scale finite element analyses were performed using two separate commercial explicit solvers. Sample comparisons of simulation results with test data will be shown here.

Keywords: Crashworthiness, Impact Dynamics, LS-DYNA, ABAQUS

BACKGROUND

NASA Langley Research Center (LaRC) is supporting the NASA Search and Rescue (SAR) Mission Office at NASA Goddard Space Flight Center (GSFC) with the Emergency Locator Transmitter Survivability and Reliability (ELTSAR) project. ELTSAR is a multi-faceted research, analysis and test effort with the ultimate goal of delivering a set of empirically-based recommendations to the Radio Technical Commission for Aeronautics (RTCA) regarding performance standards for second generation ELTs. The test phase includes a variety of experiments that are designed to evaluate ELT performance under conditions that more accurately replicate actual crash environments than those found in the current performance standard. These experiments

include drop testing, vibration, strength testing, and full-scale crash testing at the Landing and Impact Research (LandIR) facility.

LandIR is a unique facility designed to perform crash and landing tests of full-scale aircraft, rotorcraft, and spacecraft by lifting and swinging test articles using a single or double pair of cables [1]. The swing cables are connected to one end of LandIR and at hard-points on the test article. A pullback cable is connected to a movable bridge located on the opposite end and hard points on the test article. As the pullback cabling is retracted with a winch system, the aircraft is lifted to a pre-determined drop height. A pyrotechnic system severs the pullback cabling, and the test article swings along a pendulum-like flight path onto a pre-determined impact location. Just prior to impact, the swing cables are also pyrotechnically severed. The attitude and velocity at impact is determined by swing cable length, impact location, and drop height. A photo of the LandIR is shown in Figure 1.

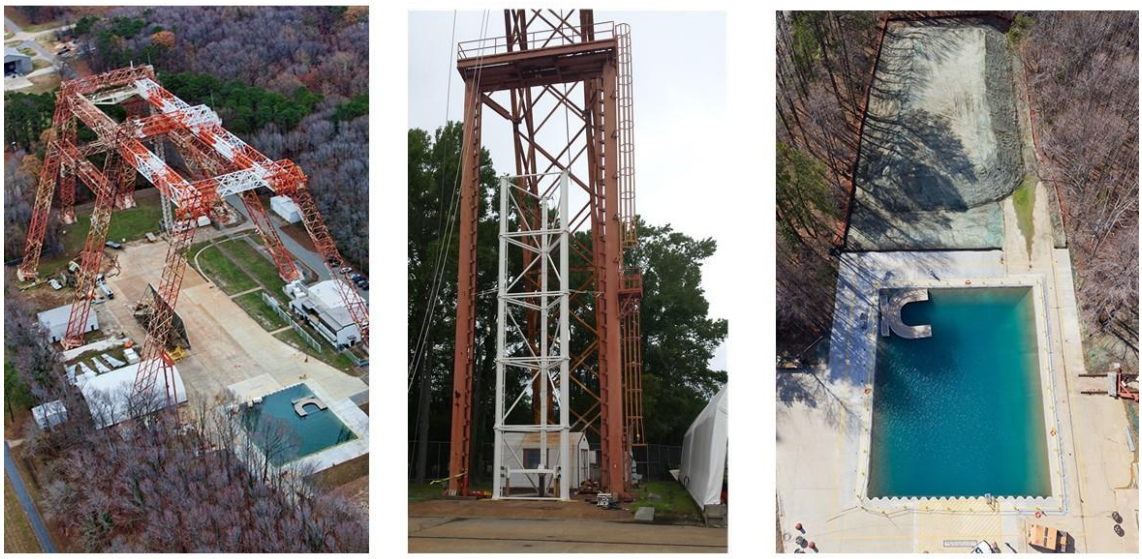

Figure 1. NASA Landing and Impact Research Facility

Since the mid-1970s the LandIR facility at LaRC has been testing General Aviation (GA) aircraft for improved crashworthiness. Tests conducted between 1974

and 1983 were used to establish Federal Aviation Administration (FAA) seat certification standards [2]. The Advanced General Aviation Transport Experiments (AGATE) program was established in the late 1990s as a collaboration between government and industry to revive the GA market. Full-scale crash tests of a Beech Starship in 1995 and a modified Lancair aircraft in 2001 were performed as technology demonstrations for AGATE [3].

A series of full-scale tests were proposed for ELTSAR using Cessna 172 general aviation aircraft. Three aircraft were acquired, and a comprehensive test series was conducted in the summer of 2015. The data from the three tests are used to correlate and calibrate structural finite element models (FEM) of the Cessna 172s. These models would then be used to predict the expected deceleration environments at various ELT locations and aircraft impact conditions. The analyses will lead to updated installation standards for the entire ELT system (beacon, antenna and interconnecting cabling).

TEST DESCRIPTION

Three Cessna high-wing, four seat, GA airplanes were purchased specifically for the test series. They are pictured in Figure 2. Test article 1 was a 1958 172 with a valid airworthiness certificate. Test article 2 was a 1958 175, which uses the 172 airframe, but contains a different engine and gearbox. The third test article was a 1975 172M with a valid airworthiness certificate. Test articles 1 and 3 were operational until the winter of 2014.

Test article 1 Test article 2 Test article 3

Figure 2. ELTSAR Crash Test Articles

Each aircraft was outfitted with similar instrumentation, cameras, and onboard experiments. The rear seats and luggage area equipment were removed from each airplane, and an onboard data acquisition system (DAS) was installed in its place. This DAS system, a time-code generator used in data synchronization, and the pyro firing system were all enclosed in a protective cage to keep the systems intact in case of severe aircraft deformation. The DAS system recorded accelerations throughout the fuselage. In addition to airframe accelerations, two 50th-percentile Hybrid II Anthropomorphic Test Devices (ATDs) were outfitted with accelerometers located in the head, chest and pelvis and load cells in the lumbar region. A seat belt load cell was used for both the pilot and co-pilot. Standard seats were used in all aircraft. Table 1 shows the channels of airframe acceleration instrumentation, and Table 2 shows ATD instrumentation. DAS data were sampled at 10 kHz.

Table 1- Airframe Instrumentation

Location	**Direction**
Engine	Longitudinal, Vertical, Lateral
Firewall	Longitudinal, Vertical
Floor under pilot seat	Longitudinal, Vertical
Floor under co-pilot seat	Longitudinal, Vertical
Cabin ceiling at aft wing	Longitudinal, Vertical
Left door frame	Longitudinal, Vertical

Right door frame	Longitudinal, Vertical, Lateral
DAS Rack (rear luggage area)	Longitudinal, Vertical
Tail	Longitudinal, Vertical, Lateral

Table 2 - ATD Instrumentation

ATD Location	**Measurement**	**Direction**
Head	Acceleration	Longitudinal, Vertical
Chest	Acceleration	Longitudinal
Pelvis	Acceleration	Longitudinal, Vertical
Lumbar	Force	Vertical
Seatbelt	Force	Strap tension

Rigging hardware was added to each of the main wing attachment points to assist with the lifting and swinging of the airframe at the LandIR facility. A single over-wing swing point was chosen as the main swing point. By selecting a single swing point, a pitch rate is introduced into each airframe which can simulate a flare, or emergency pull up condition. Hardware was also fabricated and attached at two restraint points located on the engine and the frame located at the rear of the main cockpit. The correct angle of attack was achieved by adjusting these restraint cables.

The left side of the airplane was painted with vertical and longitudinal lines and a stochastic black and white speckle pattern. This pattern aided with the collection of airframe deformation data from a technique called full field photogrammetry. Additional lead weight was added over the wing to simulate fuel weight. The lead and main swing hardware accounted for an almost full fuel load. Spoilers were attached to each wing to minimize any possible lift that would be generated as the aircraft gained speed during the swing. Finally, multiple ELTs were mounted into the cabin or tail section of each aircraft for the evaluation of their performance.

After all preparations were completed, the final weight and balance was performed on each test article, and is summarized in Table 3. The horizontal center of gravity (CG) is measured from the firewall, the lateral CG is measured from the aircraft centerline, and the vertical CG is measured from the ground. The column labelled "Moment / 1000" is calculated by multiplying the weight and horizontal CG. This number is typically found in a Pilot Operating Handbook to determine the aircraft category.

Table 3 - Aircraft Test Article Weight and CG Properties

Test	Weight	Horizontal	Lateral	Vertical	Moment / 1000	Category
1	2000	44.5	0.0	46.25	89	Normal
2	2114	39.5	0.0	48.1	101	Normal
3	2072	42.5	0.0	50.8	89	Normal

Test 1 was designed to simulate a flare to stall onto a rigid surface such as concrete. This case provided a way to isolate the airframe response for model calibration. Tests 2 and 3 were designed to simulate controlled flight into terrain conditions, where the terrain response must also be accounted for in the models. Test 2 featured the airplane impacting with a nose down condition, while Test 3 featured the airplane impact with a nose up and tail strike condition. All tests were conducted within the approximate stall speed of the aircraft. Tests 2 and 3 impacted a dirt surface consisting of a clay-sand mixture, and is known as Gantry Unwashed Sand (GUS) [4]. This soil was recently used as the impact surface for the TRACT full-scale tests [5]. Table 4 summarizes the as-measured impact conditions. For all tests, a large catch net was installed on the western side of the impact location to arrest the airplane and prevent it entering the Hydro Impact Basin located 100 feet away from the impact site. Each end of the catch net was strapped to a 5,000 lb concrete block which would slow

the aircraft to a stop. An image of the Test 1 article at the drop height is shown in Figure 3.

Table 4. Measured CG Impact Conditions

Test	Surface	Horizontal Velocity (fps)	Vertical Velocity (fps)	Flight Path Velocity (fps)	Angle of Attack (deg)	Pitch Rate (deg/sec)
1	Concrete	60.2	23	64.4	+1.48	+16.5
2	GUS	68.6	28.7	74.4	-12.2	+16.1
3	GUS	56.9	23.6	61.6	+8.0	+13.3

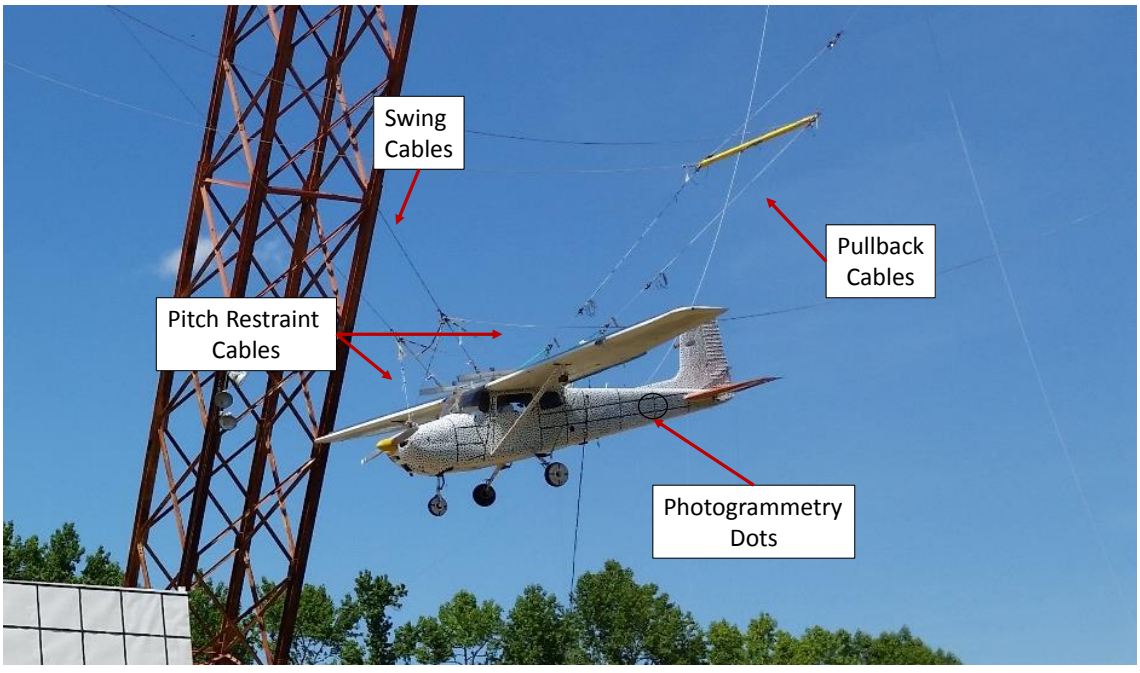

Figure 3. Test Article Swing Configuration

TEST 1 RESULTS

The airplane CG impacted the soil at 60.2-ft/sec horizontal and 23-ft/sec vertical speeds. It was pitched 1.48-degrees nose up with a pitch up rate of +16.5-degrees/second. There was approximately 0.475-seconds of time between the initial impact with the ground and the first contact of the catch net. The airframe main gear compressed almost to the point of belly impact. The pitch rotation caused the tail to strike the ground approximately 0.125-seconds after impact. The primary vertical deceleration was complete by 0.200-seconds, after which the aircraft rebounded with most its horizontal velocity maintained. The propeller first contacted the net approximately 0.475-seconds after initial impact. The catch net covered the nose and leading wing edges at approximately 0.500-seconds after initial ground impact. The 5,000-lb restraining weights attached to the catch net moved at approximately 1.120-seconds after impact. All motion stopped approximately 5.85-seconds after impact. Figure 4 shows the sequence of the ground contact, while Figure 5 shows the sequence of events for the net contact. Table 5 summarizes these events in tabular form.

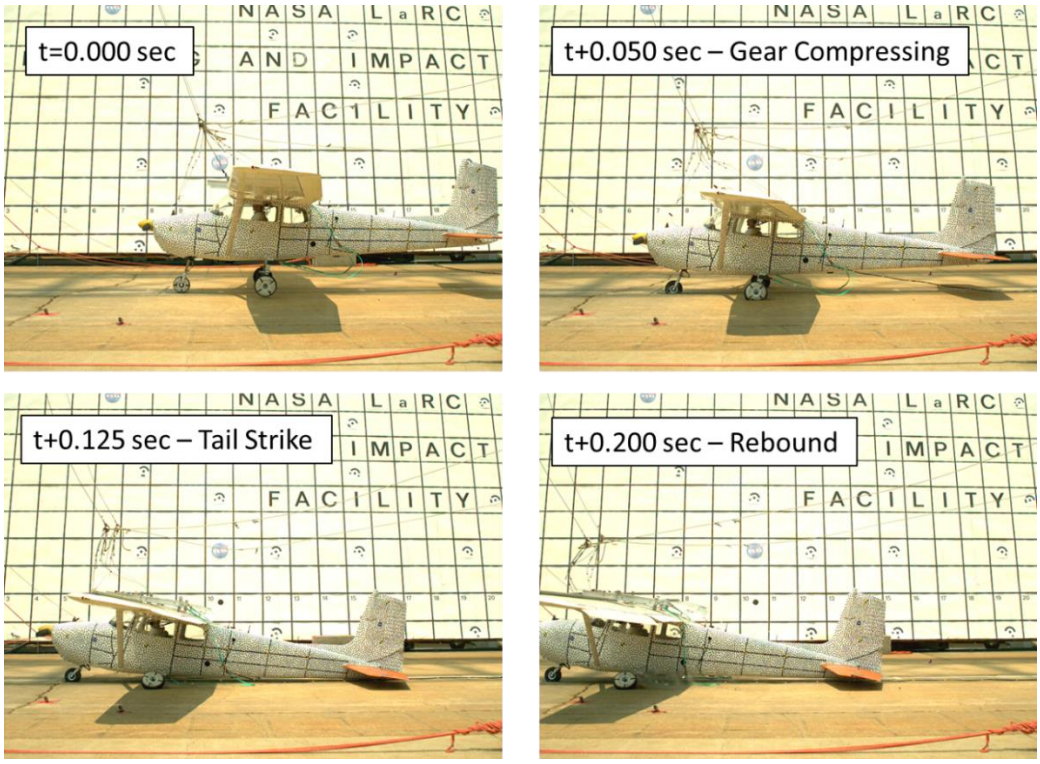

Figure 4. Test 1 Impact Sequence – Ground Contact

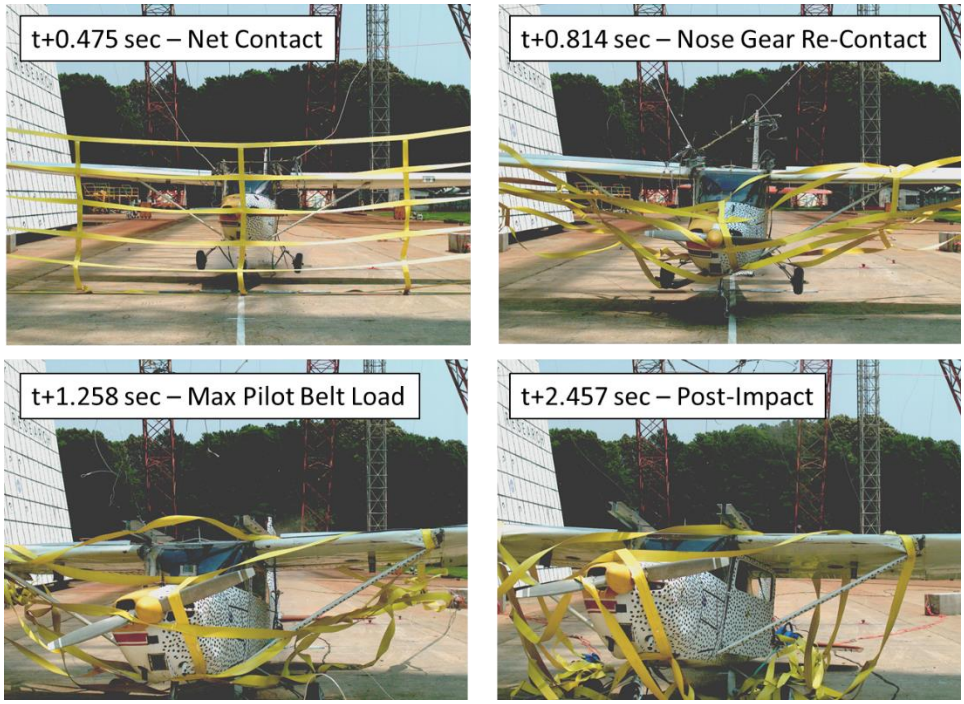

Figure 5. Test 1 Impact Sequence - Net Contact

Table 5. Event Timing for Test 1

Event	Time after impact (sec)
Nose gear impact	0.000
Main gear impact	0.006
Tail strike	0.125
Catch net contact	0.475
Second nose gear impact	0.814
Second main gear impact	0.939
Pilot door open	2.003
Motion Stop	5.835

The acceleration test results shown in Figure 6 were filtered using an SAE Channel Filter Class (CFC) 60 low-pass filter [6]. The results of Test 1 indicate a two-phase impact sequence. The first event is the airplane impacting the concrete surface, simulating a hard landing. In this event, which occurs for the first 0.300-seconds, the landing gear deforms and the plane rebounds off of the surface with minimal loss in its original horizontal velocity. The vertical acceleration shows a roughly trapezoidal shaped pulse resulting from the landing gear deflecting. Examining the plateau in acceleration occurring between 0.015-seconds (start of plateau) and 0.200-seconds (start of airplane rebound), the average sustained acceleration varies between 4.1-g in the engine to 5.9-g in the tail. The large peak in the tail is due to the tail strike, which occurred at 0.125-seconds after the impact. The horizontal acceleration at ground contact is minimal with the exception of the noise seen in the tail accelerometer, which

is due to the tail strike.

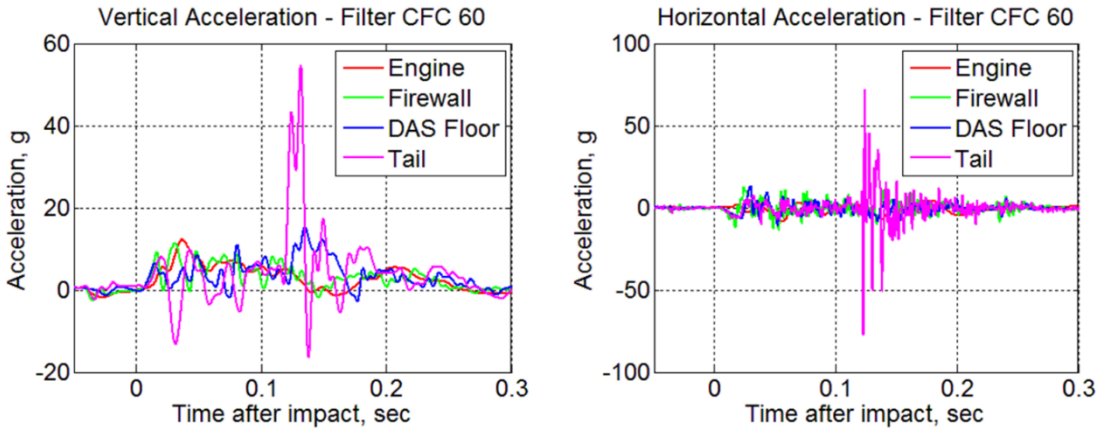

Figure 6. Test 1 Airframe Accelerations at Ground Impact

The second event is the airplane impacting the catch net. The catch net is a facility safety feature. However, when investigating the results, the catch net can simulate a real scenario such as an airplane impacting brush, berm, or other obstructions after the initial emergency/crash landing. Thus, it should be included in the data analysis in terms of its effect on the loading on the airframe and occupants. As shown in Figure 7, the horizontal acceleration in the airplane resulting from impact with the catch net was a triangular pulse shape, lasting 0.5-seconds and reaching peaks ranging between 4.0-g in the tail to 4.6-g in the nose. The large spike at the end of the net contact in the tail data is a second tail strike onto the concrete.

The heads of the pilot and co-pilot ATDs struck the yokes, but the impact loads were benign. The nose gear was partially detached. With the exception of the tail, there was no noticeable damage on the fuselage. The leading edges of the wings were damaged due to catch net engagement.

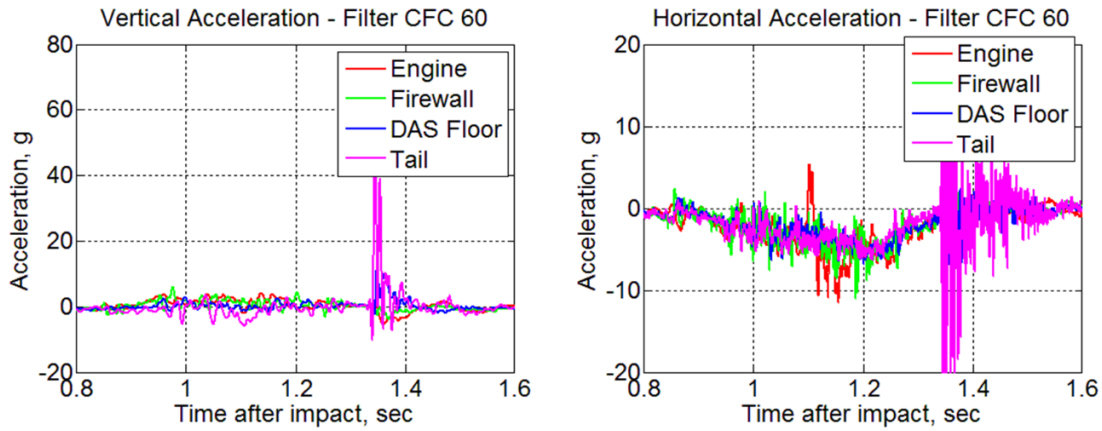

Figure 7. Test 1 Airframe Accelerations at Net Contact

TEST 2 RESULTS

Test 2 was the first of two tests where the airplane impacted a soil surface. The airplane CG impacted the soil at a 68.6-ft/sec horizontal and 28.2-ft/sec vertical speeds. It was pitched 12.2 degrees nose down with a pitch up rate of +16.1 degrees/second.

The surface of the soil was wetted using a hose approximately one hour before the test. The moisture content for Test 2 varied between 8.8% and 22.6% by weight. The density of the soil varied between 108 lb/ft^3 and 127 lb/ft^3. The bearing strength at one particular location is shown in Figure 8. The bearing strength of the soil at the surface was about 1300-lb/ft^2, and dropped to approximately 800-lb/ft^2 from a depth of 1-ft to the bottom at 2-ft.

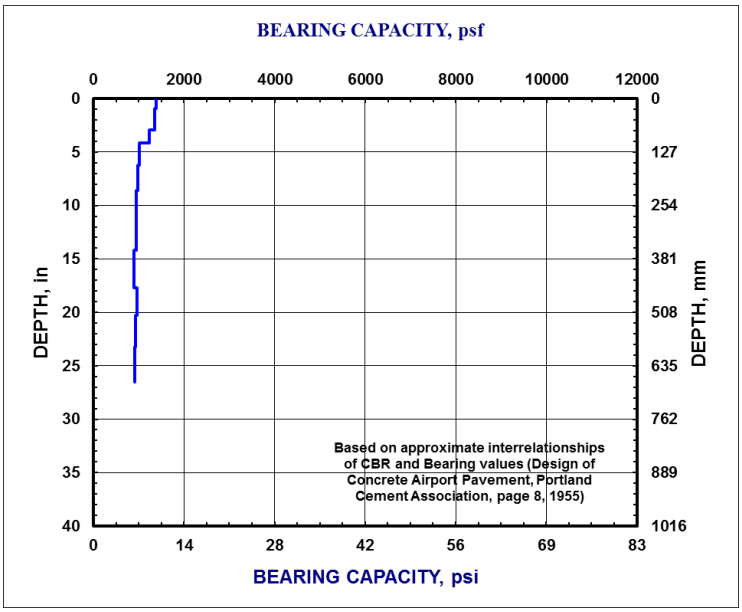

Figure 8. Bearing Capacity of the Soil in Test 2

The airplane nose gear impacted the soil first and began plowing. The nose of the airplane impacted the soil approximately 0.070-seconds after initial nose gear contact with the soil. The engine cover detached. The engine firewall buckled, with the upper engine bulkhead buckling forward and the lower engine bulkhead buckling aft. The left wing and nose gear broke away from the fuselage at around 0.10-seconds. At 0.169-seconds, the plowing caused the tail to buckle in the frame section just aft of where the floor terminates. This frame section contained an 8-inch by 12-inch side hatch opening where the buckling initiated. After 0.240-seconds the airplane started to flip over. This sequence is captured in Figure 9.

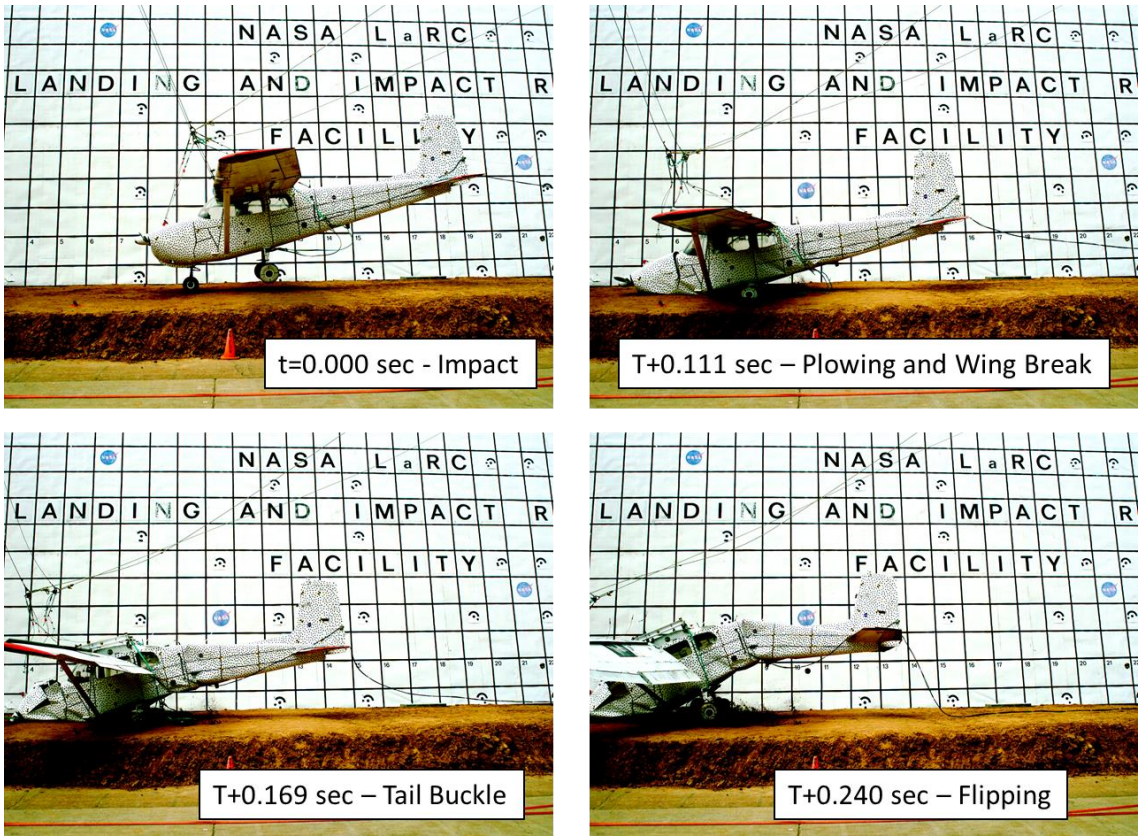

Figure 9. Test 2 Impact Sequence - Side View

The remainder of the impact was captured from an end view camera. The flipping of the airplane started at approximately 0.240-seconds after impact and the airplane landed upside-down approximately 1.976-seconds after impact. It continued to rock back and forth until it came to final rest 6.790-seconds after impact. Figure 10 shows the continuation of the impact sequence. The sequence of events that occurred during Test 2 are listed in Table 6.

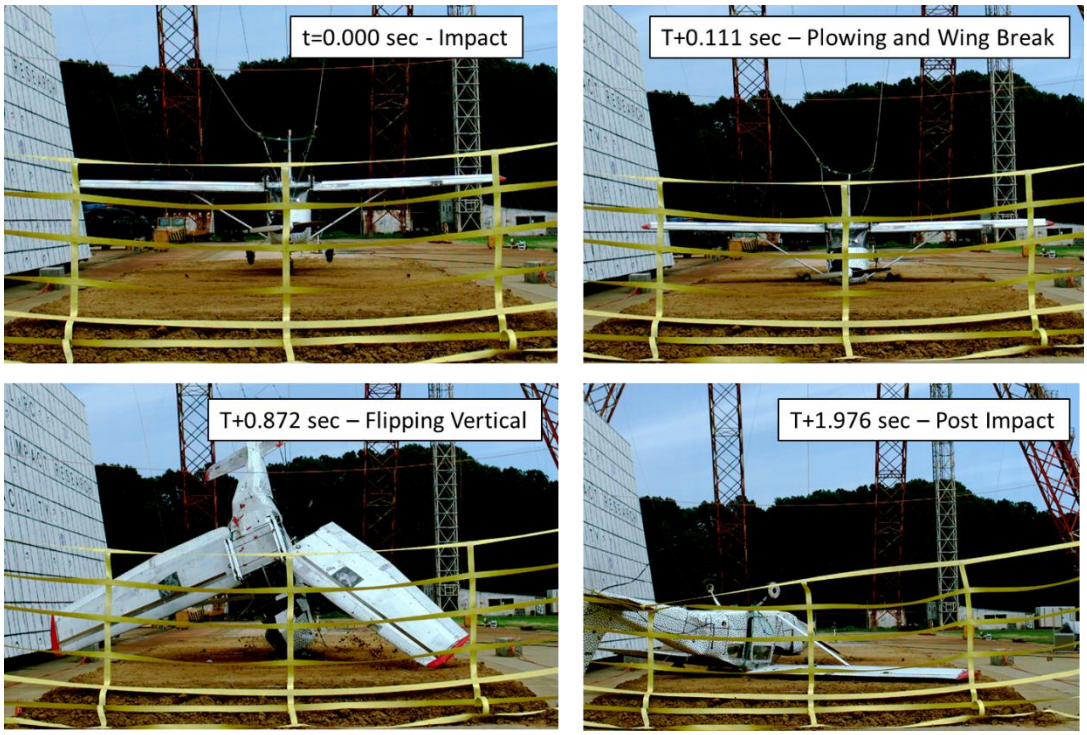

Figure 10. Test 2 Impact Sequence - End View

Table 6. Test 2 Event Timing

Event	Time after impact (sec)
Nose gear impact	0.000
Main gear impact	0.026
Nose impact	0.071
Left Wing Break	0.111
Airplane nearly vertical	1.035
Tail net contact	1.896
Motion Stop	6.790

The vertical accelerations from the different portions of the airplane are different in magnitude, duration and shape, as shown in Figure 11(a). The engine experiences a peak acceleration of less than 9-g 0.118-seconds after impact, and then the acceleration goes negative for 0.100-seconds. The cabin of the airplane is the main area which experiences peak accelerations. The pilot floor accelerometer, located in the forward

cabin, and the DAS floor accelerometer, located in the rear cabin, show peak accelerations of 23.2- and 24.6-g, respectively. The tail accelerations are almost exclusively negative during the first 0.200-seconds of the impact event. The accelerations resemble a plateau shape with an -8.2-g mean acceleration, lasting 0.130-seconds. The tail continues on a downward trajectory, before the airplane starts rotating after 0.240-seconds.

The horizontal accelerations in Figure 11 show similar responses for both shape, magnitude and duration for all locations, with the exception of a large spike in the DAS floor. Engine acceleration is not plotted due to a severed cable which resulted in signal loss from that location. The horizontal acceleration resembles a 0.130second triangular pulse with peaks of 18.6-, 39- and 13.5-g. for the pilot floor, DAS floor (rear cabin) and tail, respectively.

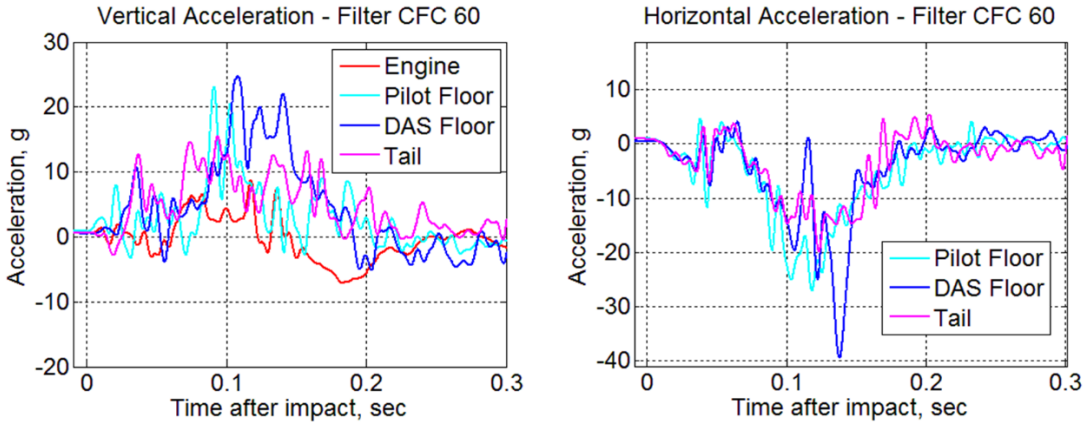

Figure 11. Test 2 Airframe Accelerations

The pilot ATD was restrained with a lap belt, and the co-pilot was restrained with a Y-harness. The high horizontal acceleration caused the lap belted ATD head to impact the dashboard, and the loads exceeded the Head Injury Criteria (HIC) limits of 1,000 [7]. The Y-harness failed, but the HIC for that ATD did not exceed 1,000. Post-test examinations of the seats revealed both rear seat rail attachments were either

partially or fully pulled out from the seat track. All four of the front seat attachments were set normally in the seat track.

TEST 3 RESULTS

The same soil surface from Test 2 was used. The surface was tilled on the day of the test to remove any compaction that may have occurred due to personnel walking on it leading up to the test day. The dirt was not wetted down immediately prior to the crash test.

The moisture content for Test 3 varied between 11% and 14% by weight. The density of the soil varied between 138-lb/ft^3 and 152-lb/ft^3. The bearing strength was very similar to Test 2. The bearing capacity as a function of depth is shown in Figure 12.

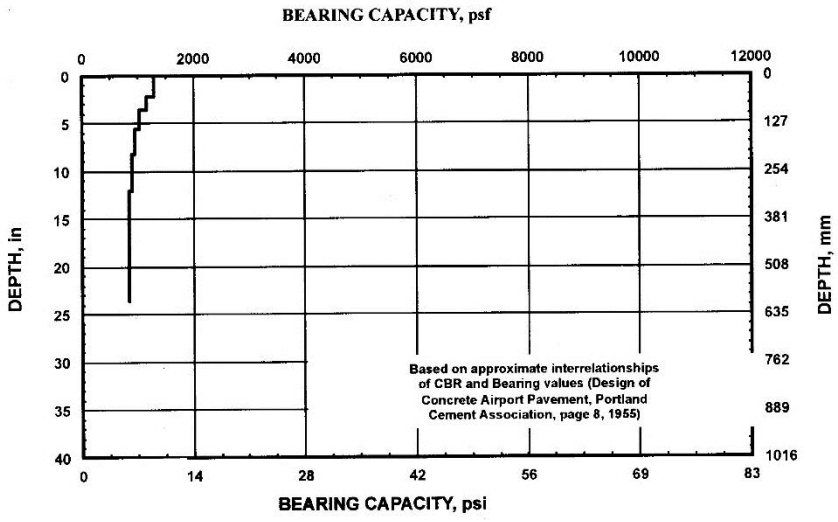

Figure 12. Test 3 Soil Bearing Capacity

The airplane CG impacted the soil at a 56.9-ft/sec horizontal and 33.6-ft/sec vertical velocities. It was pitched 8-degrees nose up with a pitch rate of +13.3-deg/sec. There was a slight amount of roll (right side high) and yaw (nose left) to the test article for Test 3.

The impact sequences from the side cameras and end cameras are shown in Figure 13 and Figure 14, respectively. The sequence of events that occurred during Test 3 are listed in Table 7. Due to the slight amount of roll and yaw, the airplane left main gear impacted the soil first. As the tire and the gear deformed, the tail contacted the surface at 0.030-seconds. The nose gear, along with the nose of the airplane contacted the surface at 0.116-seconds. As with Test 2, after the nose gear penetrated into the soil surface the airplane began to rotate about the nose. Unlike Test 2, however, the tail developed a fracture aft of the frame section where the floor terminates at 0.138-seconds after the initial impact. The fracture initiated below the aft window and propagated along the sidewalls, causing the tail to almost break free of the fuselage. A small portion of skin on the bottom of the aircraft held the tail to the rest of the airplane during the rotation. The rotation of the aircraft lasted until approximately 1.53-seconds after the impact, at which time the ceiling of the airplane contacted the soil. The airplane rocked for a few seconds before finally coming to rest at almost 5-seconds after initial impact.

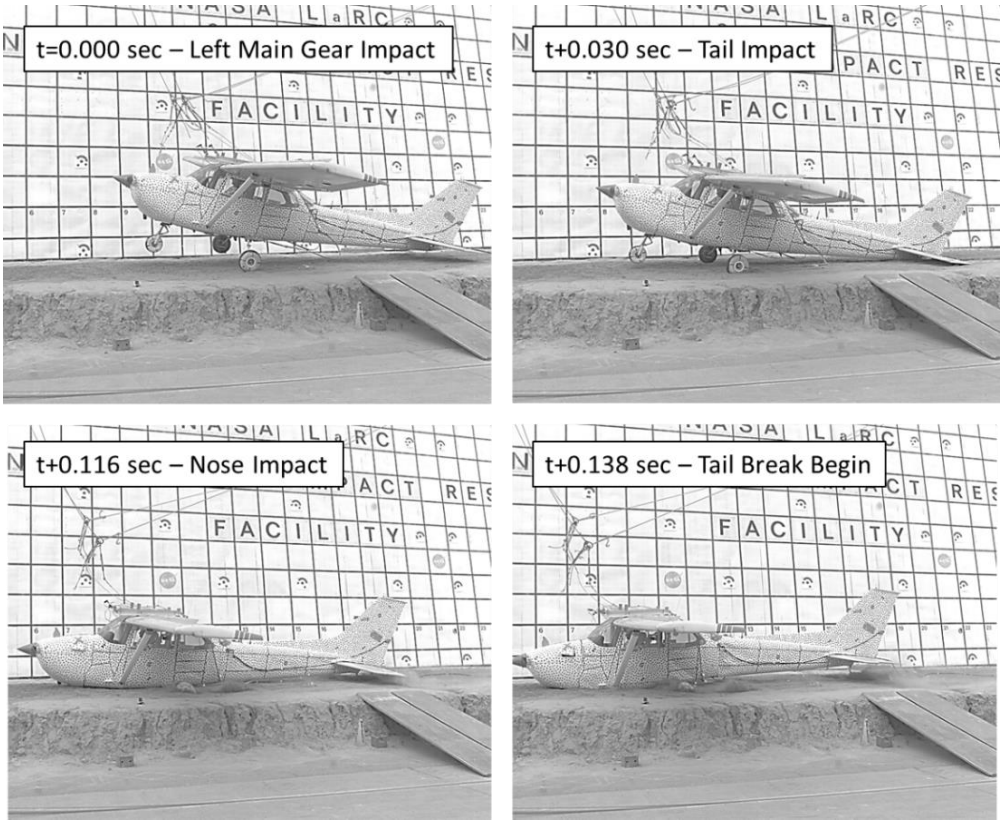

Figure 13. Test 3 Impact Sequence - Side View

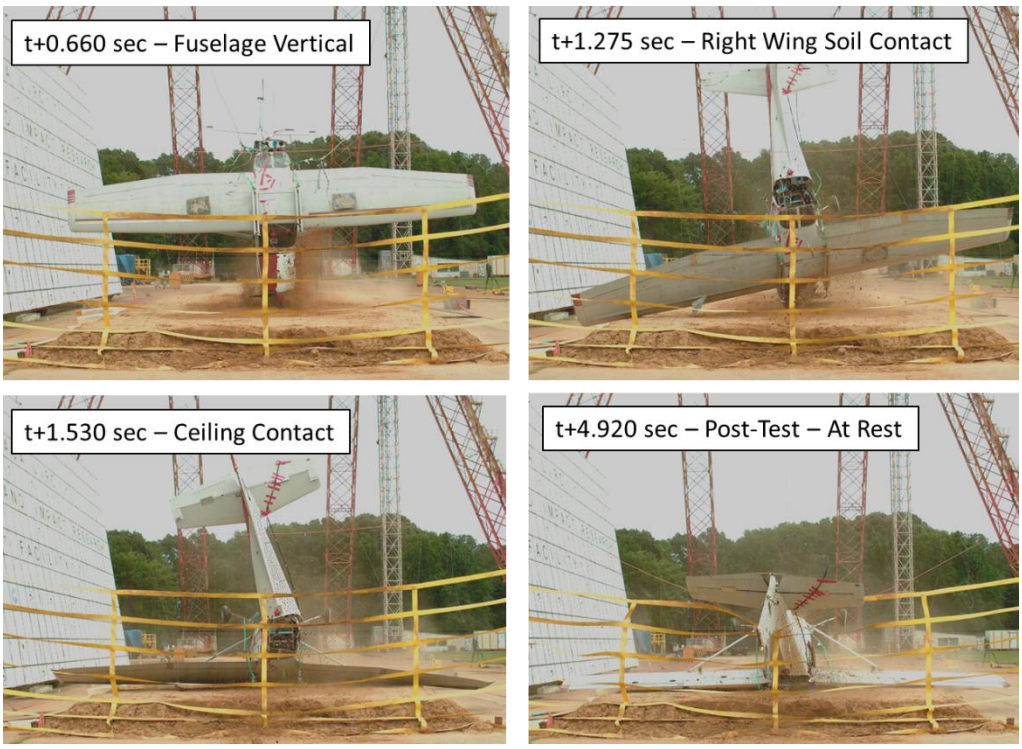

Figure 14. Test 3 Impact Sequence - End View

Table 7. Test 3 Event Timing

Event	Time after impact (sec)
Left main gear contact	0.000
Tail contact	0.030
Nose contact	0.116
Tail break begin	0.138
Fuselage Vertical	0.660
Ceiling contact (upside-down)	1.530
Motion stop	4.920

Figure 15 shows the airframe accelerations. A slap-down effect can be seen in the vertical acceleration plots. The tail strike is first captured by the instrumentation approximately 0.080-seconds after initial impact and reaches a peak of approximately 34-g. The peak accelerations are staggered and move from the aft end forward. These accelerations reach their peaks between 0.165 and 0.206-seconds after first contact of the DAS floor, firewall and engine, respectively. The vertical acceleration pulses for all locations last for approximately 0.240-seconds.

The horizontal accelerations resemble either a triangular or trapezoidal pulse shape, depending on the location, as shown in Figure 15. The engine acceleration peaks at 22.2-g at 0.210-seconds, shaped over a 0.180-seconds triangular pulse. The firewall peak acceleration was 38.9-g; however, this peak is likely due to the increased noise in the signal from the firewall location. The peak occurs at 0.165-seconds after impact and the shape also resembles a 0.180-second triangular pulse. The DAS floor and tail accelerations represent a trapezoidal-shaped pulse, having a 0.050-seconds sustained acceleration and a total pulse width of 0.250-seconds. The DAS floor sustained acceleration is approximately 8.7-g, while the tail reaches a sustained acceleration of 8.1-g. The sustained accelerations are caused from the dragging of the airplane through

the dirt before rotation around the nose gear tire begins, and occur mainly in the rear portions of the airplane due to the tail strike condition.

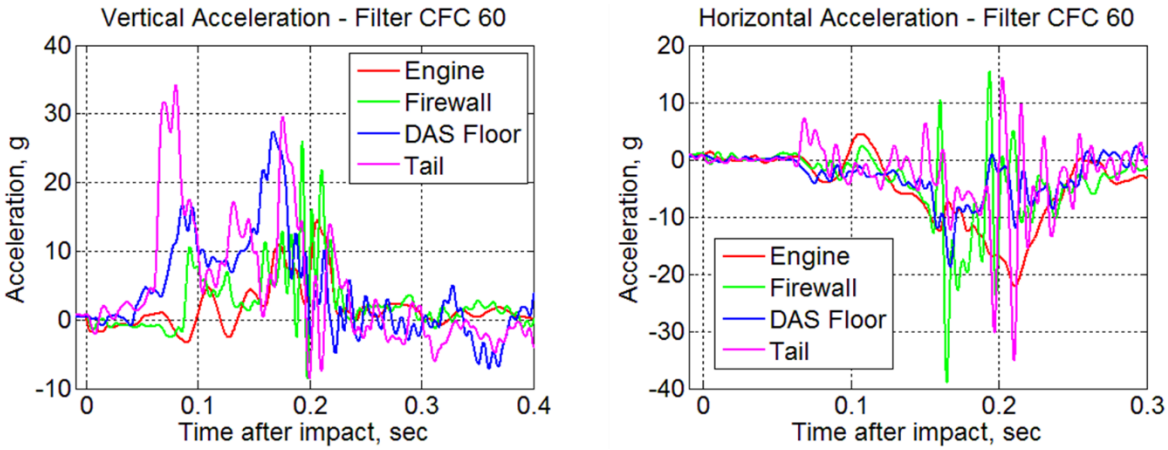

Figure 15. Test 3 Airframe Accelerations

MODEL DEVELOPMENT

Analysis Solvers

In addition to experimental evaluation of ELT performance, a major objective of this research program was to develop finite element models of the C-172 airframes independently using two different commercial codes, and to validate the models through extensive test-analysis correlation. Two nonlinear explicit, transient dynamic finite element (FE) codes were selected, LS-DYNA [8] and ABAQUS/Explicit [9]. LS-DYNA is marketed by Livermore Software Technology Corporation (LSTC) and is widely used for automotive crash simulations. ABAQUS/Explicit is marketed by SIMULIA under its parent company Dassault Systèmes, and is widely used for drop tests, crushing, and simulation of manufacturing processes. Two finite element codes were chosen for test correlations because different codes have specific approaches for model development and calibration. Modeling aspects that must be considered for each code include landing gear representation, mesh refinement for the airframe, soil

constitutive parameters, contact algorithms, and distribution of non-structural mass to match the mass and CG of the test article. The three ELTSAR tests that varied in crash severity provided a unique opportunity to assess the advantages and limitations for each code.

Geometry for Analytical Models

Development of the FE models was complicated by the fact that no prior geometry or static load models of the C-172 airframe existed and no engineering drawings were available. Consequently, an original CAD (computer aided design) geometry of the airframe was generated using both a three-dimensional laser scan and hand measurements of the test article. The measurements were used as inputs to the Conceptual Design Shop (CDS) tool, an airframe geometry generation tool developed within the PATRAN FE modeling software [10]. Initial geometry from CDS was tuned to match the point cloud from the laser scan, as shown in Figure 16. The CDS-generated geometry included internal structure (ribs, spars, frames, etc.) of the airframe. The FE models for both codes were discretized from this common model, although several additional structural components (ELTs, point masses, LandIR mounts) were later added independently by each analysis team.

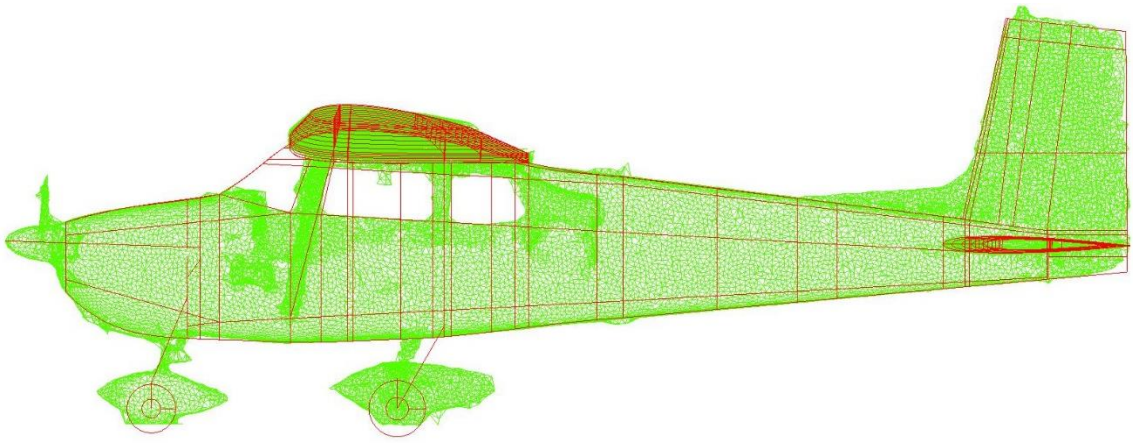

Figure 16. Test 1 CDS geometry (red) and Laser Scanned Data (green)

Simulations for the Test 1 and 2 configurations used the same FE airframe model. For the Test 3 simulations the fuselage aft of frame 108 was replaced with the swept tail geometry, as shown in Figure 17. The LS-DYNA team generated the aft fuselage geometry for the Test 3 model from a laser scan point cloud. For the ABAQUS model, the CDS geometry was used.

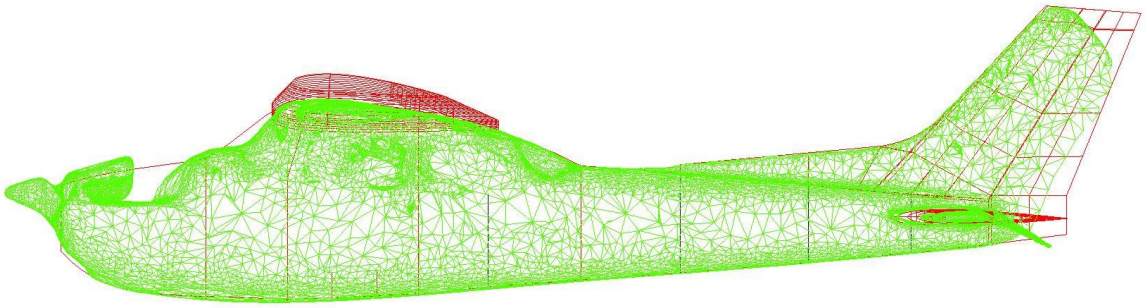

Figure 17. Test 3 CDS geometry (red) and Laser Scanned Data (green)

TEST AND ANALYSIS COMPARISONS

LS-DYNA Test 1 Simulation

The model representing the Test 1 configuration is shown in Figure 18. This model contains 135,643 nodes; 252 beam elements; 139,974 shell elements; 908 solid elements; 1 discrete beam; 44 parts; 8 Constrained Nodal Rigid Bodies (CNRBs); 11 different materials; 1,524 concentrated masses; 1 card defining gravity; and 1 rigid wall. All nodes forming the aircraft model were assigned the same initial velocity conditions, as measured for the test. In addition, a pitch angular velocity of 16.5-degrees/second was assigned about the CG of the model representing the measured condition. The aircraft was also pitched by 1.5-degrees (nose up) to match the orientation of the test article at impact. The concrete impact surface, which is not depicted in Figure 18, was modeled as a horizontal rigid wall, located just below the model. Most of the shell elements used in the model were assigned a Belytschko-Tsay (Type 2) formulation;

however, the shell elements forming the main gear leaf spring were assigned a fully integrated formulation (Type 16). A nominal shell element edge length of 1-in. was used. In addition, the four ELTs were included in the model and they were represented as rigid boxes made of solid elements. The wing fuel, engine, nose cone, propeller, DAS box, two seats, and the two dummy occupants were simulated as concentrated masses. The model was executed for 0.25-seconds on a Linux workstation computer with 8 processors, running LS-DYNA V971 R712 SMP double precision, and required 5 hours and 10 minutes clock time to reach normal termination. Nodal output requests for the simulation included acceleration- and velocity-time histories at locations matching accelerometers mounted in the test article.

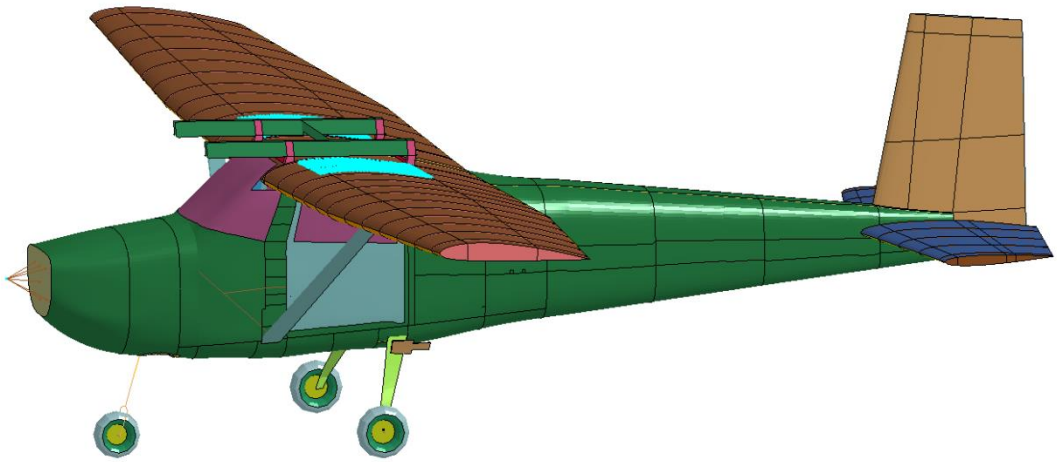

Figure 18. Test 1 LS-DYNA Model

Several pre-test simulations were executed to evaluate the integrity of the model. The model weight was within 20-lb of the 2,000 lb test weight, and the CG locations with within 2-5 inches. These results are an indication that the model represented the inertial properties of the test article reasonably well. As indicated in the Test Results section of the paper, Test 1 essentially represented a “hard” landing. Initially, the nose

gear tire impacted the concrete, followed closely by impact of the main gear tires. The main landing gear spread outward, as the nose gear stroked vertically approximately 8-in. during the test. The only fuselage contact with the impact surface was a slight impact of the rearmost portion of the lower tail. After this impact, the airframe rebounded upward and was caught by the safety net. Thus, it became apparent following the test that capturing the behavior of the nose and main gear were essential to accurate prediction of the response.

A sequence of photographs taken from the high-speed camera is shown in Figure 19, along with corresponding views of the model deformation. The photographs show a side view of test article motion and deformation occurring during initial impact. Note that the safety net is not visible in the photographs. In general, the model accurately captures the kinematic response.

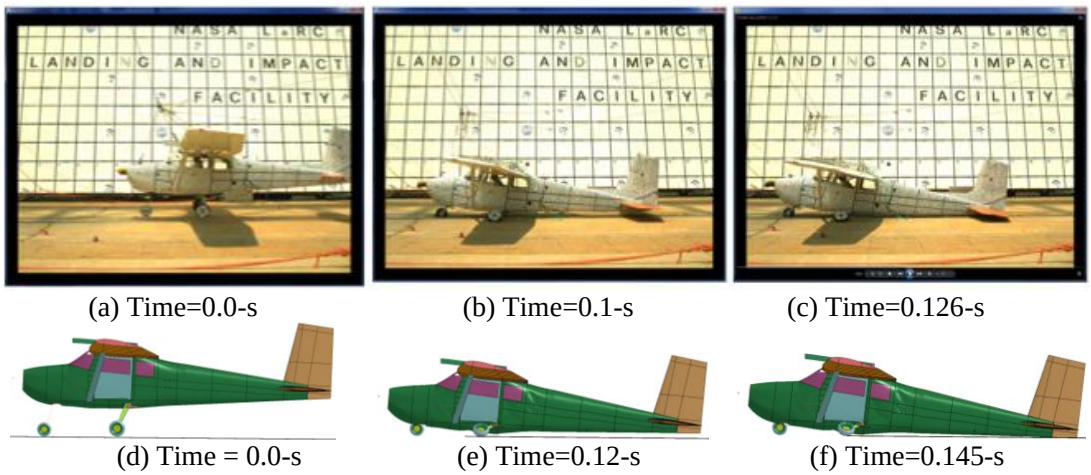

(a) Time=0.0-s (b) Time=0.1-s (c) Time=0.126-s

(d) Time = 0.0-s (e) Time=0.12-s (f) Time=0.145-s

Figure 19. Test 1 Time Sequence of Test and LS-DYNA Analysis Deformation

Next, time history comparisons are presented for various locations in the airframe. For these plots, the test and analytical data were filtered using an SAE Channel Filter Class (CFC) 20 low-pass filter [6]. Vertical acceleration responses of the pilot and co-pilot floor are plotted in Figure 20. The test responses are extremely low in

magnitude, averaging about 5-g. The predicted responses exhibit more oscillations than seen in the test data; however, the average acceleration is approximately the same as the test, 5-g. The analytical responses indicate a 13-g peak near the end of the pulse, just after 0.15-seconds. During the test, the tail section impacted the ground at 0.125-seconds. For the model, this impact occurred at 0.145-seconds. This event produced the peaks seen in the predicted responses; however, similar responses were not seen in the test. This finding indicates that the tail impact was a less severe event during the test than in the simulation.

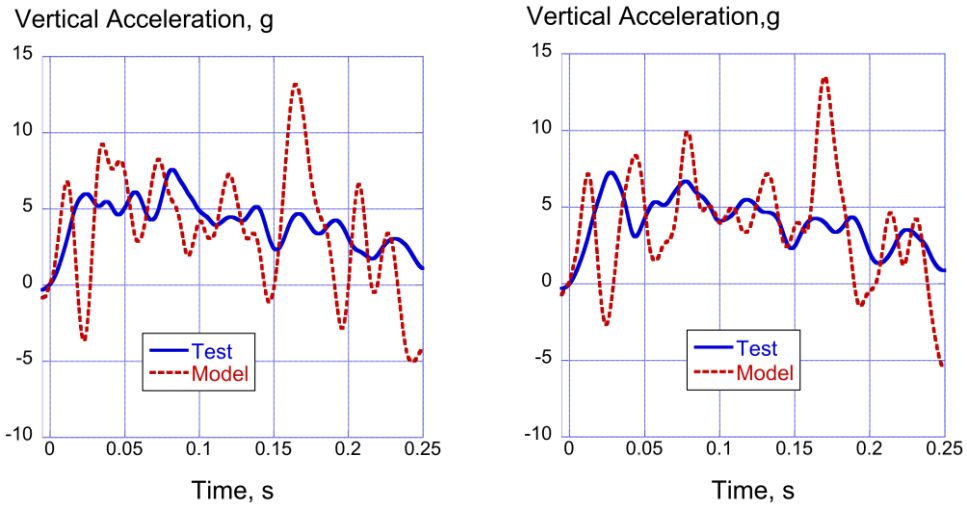

(a) Pilot floor responses. (b) Co-pilot floor responses.

Figure 20. Test 1 Pilot and Co-Pilot Floor Level Acceleration Responses

Finally, plots of vertical acceleration are shown in Figure 21 comparing test and predicted responses at three locations: the engine mass located at the front of the airframe, the DAS box located at the mid-cabin, and the center of the rear bulkhead located near the tail section. Both the test and analytical responses were filtered using a SAE CFC20 low-pass filter [6]. The engine responses, shown in Figure 21(a), are generally low in magnitude. The test response exhibits an early 12-g peak, and a fairly significant reduction in acceleration following 0.12-s. The predicted engine response contains more oscillations than seen in the test data; however, the overall magnitude of

the predicted response matches the test data quite well. The analysis also predicts a dip in the acceleration response beginning at .012-s. The dip in acceleration is attributed to the overall heaving motion of the engine during the test. The test and analytical DAS box and rear bulkhead responses, shown in Figure 21(b) and (c), respectively, are similar in that both exhibit low magnitude accelerations, on the order of 5- to 10-g, during the first 0.125-s of the response. For the test, at 0.125-s, the acceleration responses build to a peak of 12.5-g for the DAS box and 37-g for the rear bulkhead. The predicted peak is higher in magnitude for the DAS box at 14.5-g, but is lower for the rear bulkhead at 31-g. The predicted peak accelerations lag in timing compared with the test results by 0.025-s. The peaks that occur late in the acceleration responses are attributed to the tail impact

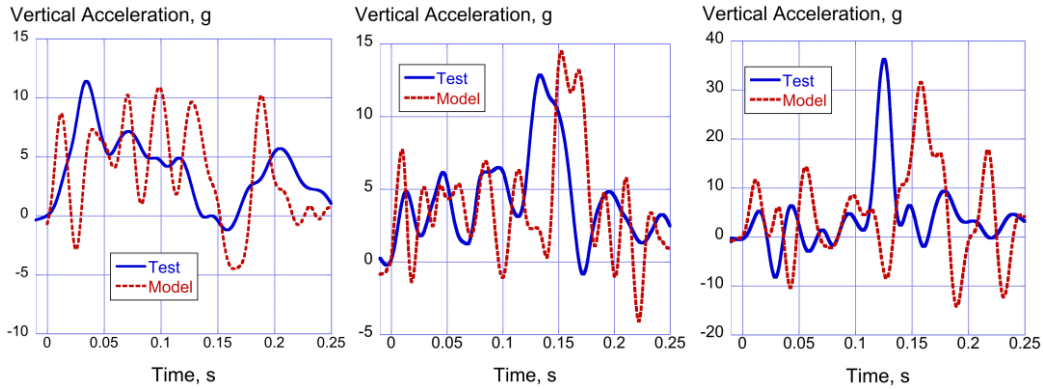

(a) Engine. (b) DAS Box. (c) Rear bulkhead.

Figure 21. Test 1 LS-DYNA/Test Accelerations at Engine, DAS Box, and Rear Bulkhead

LS-DYNA Test 2 Simulation

The model used to represent Test 2 is shown in Figure 22. The model consists of: 356,319 nodes; 140,064 shell elements; 249 beam elements; 204,583 solid elements; 47 parts; 10 CNRBs; and, 11 material cards. Several changes were made to this model including replacing the rigid wall in the Test 1 model with a soil bed constructed of solid elements, the occupant masses were moved forward by 10-in. to match the test

condition, and an 8-in. x 12-in. hole was created on one side of the tail section to represent the hole produced by a thin access panel that was not secured to the airframe and that popped off upon first impact. A special material model was assigned to the soil to represent a relatively hard gantry soil. Other changes made to the model included the addition of a fifth ELT, the addition of an automatic single surface contact, and changes to the mesh of the engine cowling that allowed it to separate during the impact event. Note that in the previous Test 1 model, the contact was input using the rigid wall definition. Finally, for Test 2, the nose gear was essentially locked into place. Consequently, the nose gear in the model was fixed.

All nodes forming the aircraft model were assigned the same initial velocity conditions, as measured for the test (823.2-in/s forward velocity and 344.4-in/s vertical velocity). In addition, a pitch angular velocity of 16.1-degrees/second was assigned about the CG of the model representing the measured condition. The aircraft was also pitched by 12.2° (nose down) to match the orientation of the test article at impact. As with the Test 1 model, the wing fuel, engine, nose cone, propeller, DAS box, two seats, and the two dummy occupants were simulated as concentrated masses. The model was executed for 0.6-s on a Linux workstation computer with 8 processors, running LS-DYNA V971 R712 SMP double precision, and required 10 hours and 40 minutes of clock time to reach normal termination. Nodal output requests for the simulation included acceleration- and velocity-time histories at locations matching accelerometers mounted in the test article.

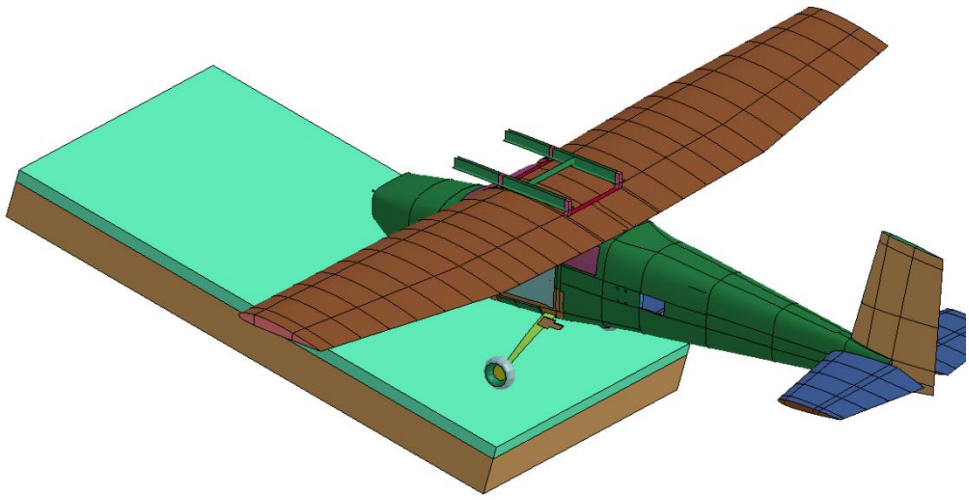

Figure 22. Test 2 LS-DYNA Model

Time sequence depictions showing model deformation and kinematics are shown in Figure 23. The sequence shows that the model predicts that the nose gear becomes buried in the soil by 0.04-seconds and by 0.08-seconds the nose gear has failed. At 0.08-s, evidence of tail buckling is observed, which continues through 0.2-seconds. Downward bending of the tail section is observed at 0.16-seconds. By the end of the simulation at 0.6-seconds, the aircraft is oriented vertically upright. In general, the model does not predict permanent damage as severe as seen during the test, and it does not predict separation of the left wing. Also, the model seems to predict the occurrence of events much faster than the test. For example, in the test the aircraft is oriented vertically (perpendicular to the soil surface) at 1.035-seconds, whereas the model has achieved this position by 0.6-s. However, separation and failure of the engine cowling and damage to the nose cone is well predicted.

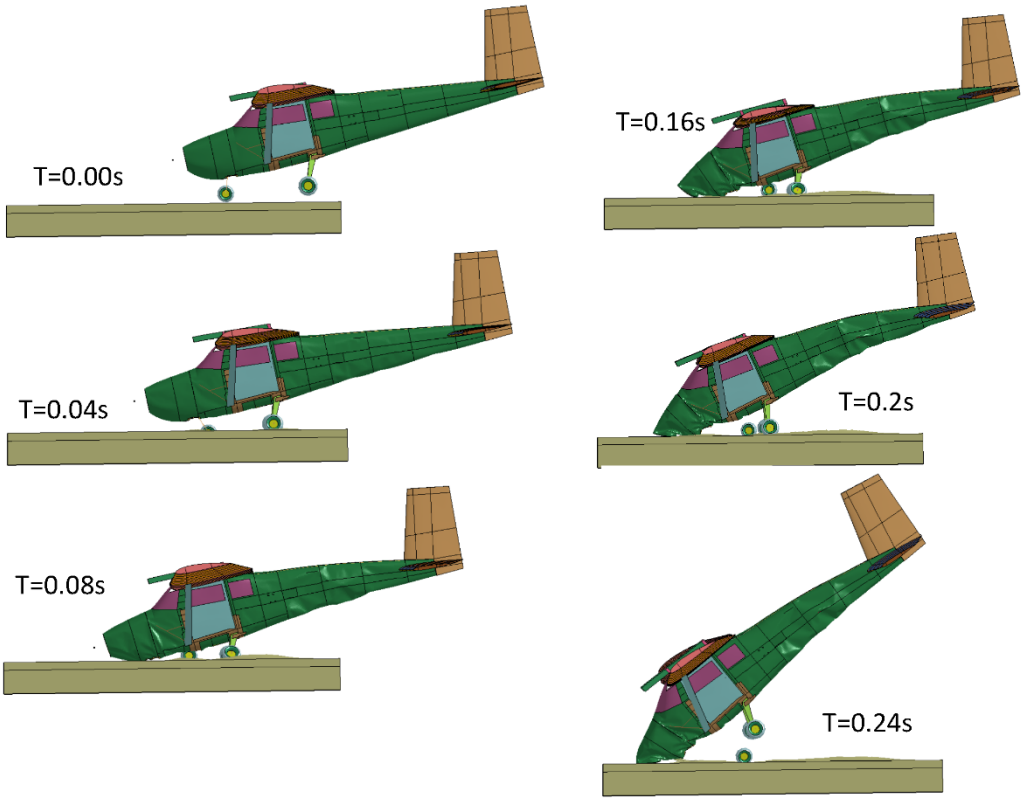

Figure 23. Test 2 LS-DYNA Predicted Model Kinematic Time Sequence

A fringe plot of predicted vertical displacement of the soil is shown in Figure 24(a), compared with a post-test photograph showing the soil deformation pattern in Figure 24(b). The model matches the overall shape of the deformation pattern. The predicted location of maximum soil displacement matches the test data, as well; however, the maximum displacement of the model (8.73-in.) is lower than the measured maximum of 11-inches. This finding is an indication that the soil model, which represented hard gantry soil, may be too stiff.

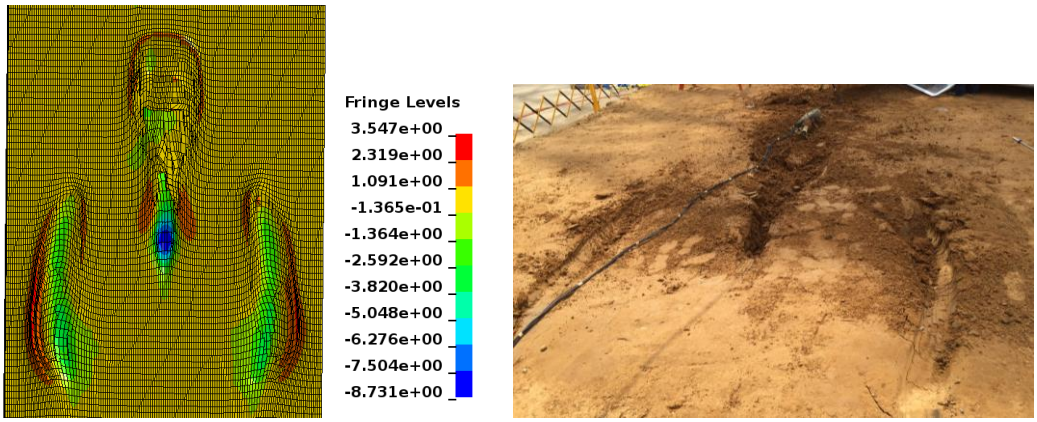

(a) Fringe plot of soil vertical deformation. (b) Post-test photograph of soil.

Figure 24. Test 2 LS-DYNA/Test Soil Deformation

Due to severe damage experienced by the nose cone and tail sections, comparisons of time history responses for Test 2 are limited to the cabin area. Plots of forward and vertical acceleration responses at the co-pilot floor location are shown in Figure 25(a) and (b), respectively. For the forward accelerations, the test data indicate a triangular-shaped pulse with a peak acceleration of 25-g. The model does an excellent job of predicting this response. For the vertical accelerations, the test response shows a small initial acceleration followed by a larger peak of 15-g magnitude. The predicted vertical acceleration response clearly demonstrates two peaks, the first one generally lower in magnitude than the second. The initial peak in the predicted response occurs while the test data shows a small initial oscillatory response. The overall magnitude of the second predicted peak response shows generally good agreement with the test response.

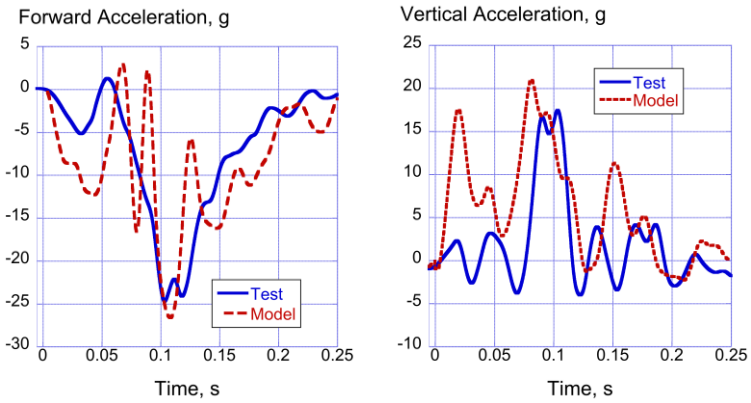

(a) Forward acceleration (b) Vertical acceleration

Figure 25. Test 2 LS-DYNA/Test Accelerations at Co-Pilot Floor

Plots of forward and vertical acceleration responses at the left doorframe location are shown in Figure 26(a) and (b), respectively. For the test, the forward acceleration indicates a triangular-shaped pulse with a peak acceleration of approximately 25-g. The model predicts a similar response for the forward acceleration, though the magnitude of the peak is lower than the test. As before, the experimental vertical accelerations show an initial small oscillatory response (less than 5-g), followed by a single large peak of 26-g magnitude. In contrast, the predicted response contains two peaks with the first being smaller in magnitude than the second. Generally, the second peak in the predicted responses matches the timing of the single large peak in the test responses.

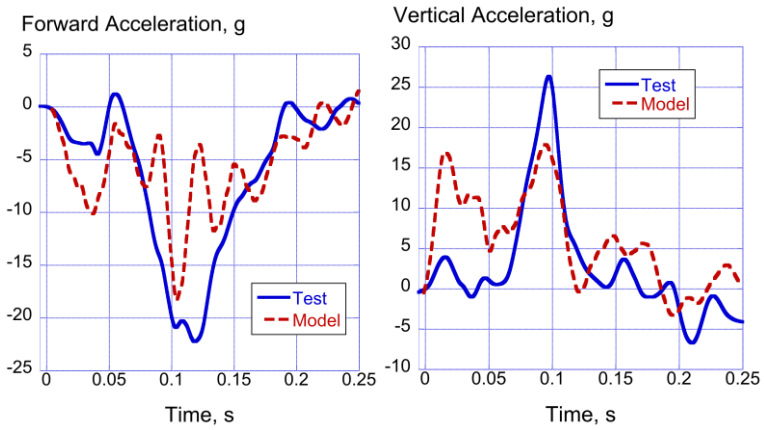

(a) Forward acceleration (b) Vertical acceleration

Figure 26. Test 2 LS-DYNA/Test Accelerations at Left Doorframe

LS-DYNA Test 3 Simulation

Considerable modifications were required to construct the Test 3 model due to the presence of the swept tail. As before, a laser point cloud was generated of the new tail section that was converted to a geometry file, which was then discretized into a finite element model. The LS-DYNA model is depicted in Figure 27. Note that portions of the model from the end of the wing forward are the same as in Test 2; however, aft of the wing represents the new portions of the model. The nose gear in the Test 3 model was the same telescoping nose gear used in the Test 1 model. However, this configuration of the aircraft contained a new main landing gear that was constructed of steel tubes. In the Test 3 model, the steel tubes were represented using beam elements. Preliminary simulations and model validation are being performed and will be presented in a future paper.

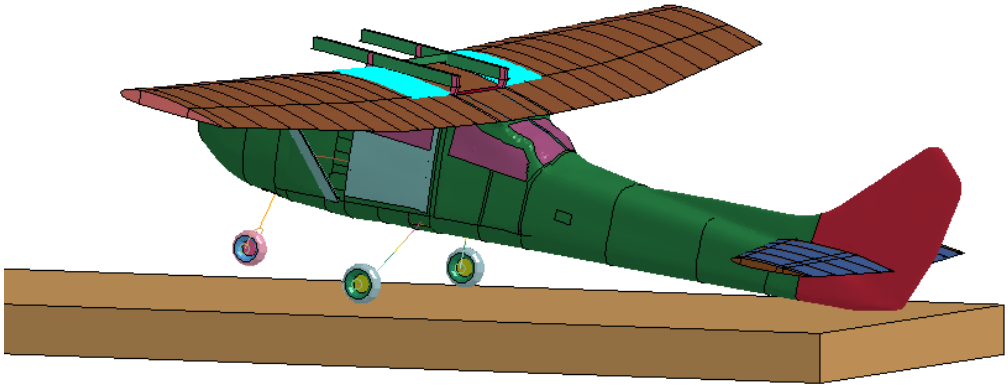

Figure 27. Test 3 LS-DYNA Model

ABAQUS Test 1 Simulation

The ABAQUS model representing the Test 1 configuration is shown in Figure 28. A nominal shell element edge length of 1.5-in. was used. This model contains 98,177 nodes, 191 beam elements, 72,827 shell elements, 848 solid elements, 37 multi-point constraints, 8 different materials, 4 revolute connectors (wheel axles), and 19 concentrated masses. Four point masses (totaling 110-lb) were added to the model to match the weight and CG (within 0.25-inches) of the test article. The shock absorber in the nose landing gear is represented by a slot connector element using the load displacement curve shown in Figure 29. The concrete impact surface was modeled as a horizontal rigid shell element, located 0.1-inches below the model. All shell elements were defined as ABAQUS S3R and S4R elements, and beam elements were defined with ABAQUS B31 elements. The four ELTs, DAS box, and tires were modeled as C3D8 solid elements. The wing fuel, engine, seats, and dummy occupants were simulated as concentrated masses. The model required 3.3 hours of wall clock time on an 8-processor Windows 7 workstation using ABAQUS/Explicit version 6.12 to simulate 0.25-seconds of impact. Nodal acceleration- and velocity-time histories at accelerometer locations were extracted from the results file.

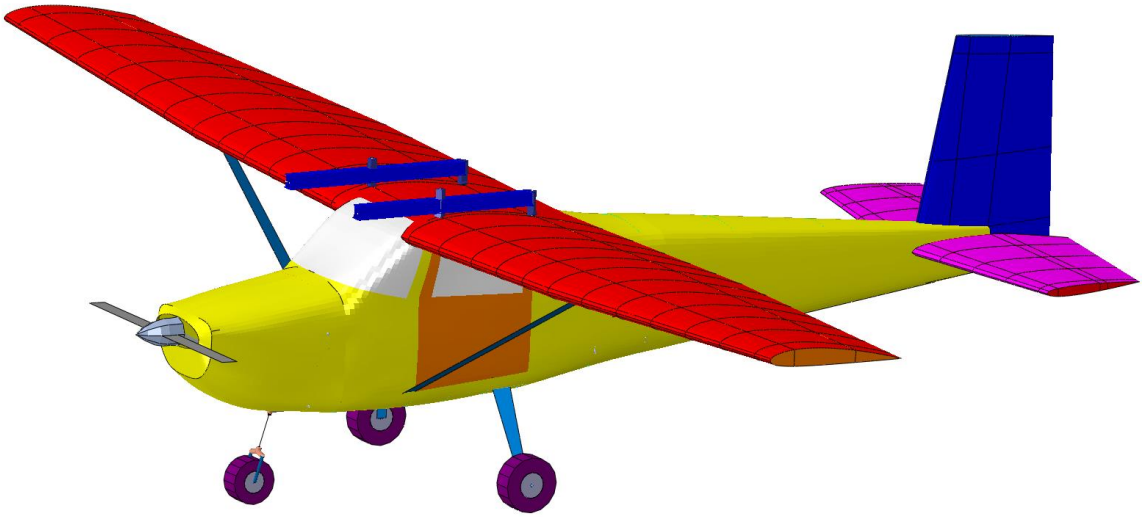

Figure 28. Test 1 ABAQUS Model

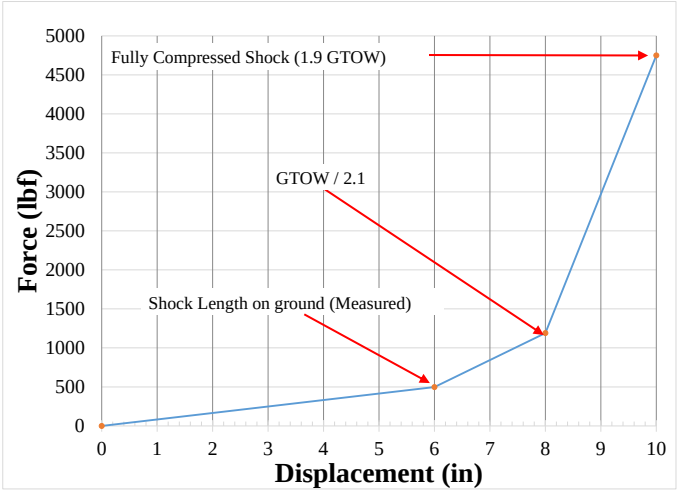

Figure 29. Derived Load-Displacement Curve for Nose landing Gear Shock

A sequence of photographs taken from the high-speed camera is shown in Figure 30, along with corresponding views of the matching model kinematics. Time history comparisons are presented for various locations in the airframe. For all ABAQUS plots, the test and analytical data were filtered using an SAE Channel Filter Class (CFC) 20 low-pass filter [6]. Vertical acceleration responses at three locations (the engine, the DAS box, and the tail) are plotted in Figure 31. The model shows significant oscillation within the structure, and higher acceleration response magnitudes. Differences in the simulation and test are most likely caused by uncertainty in the stiffness of the nose gear

shock and the stiffness of the tires.

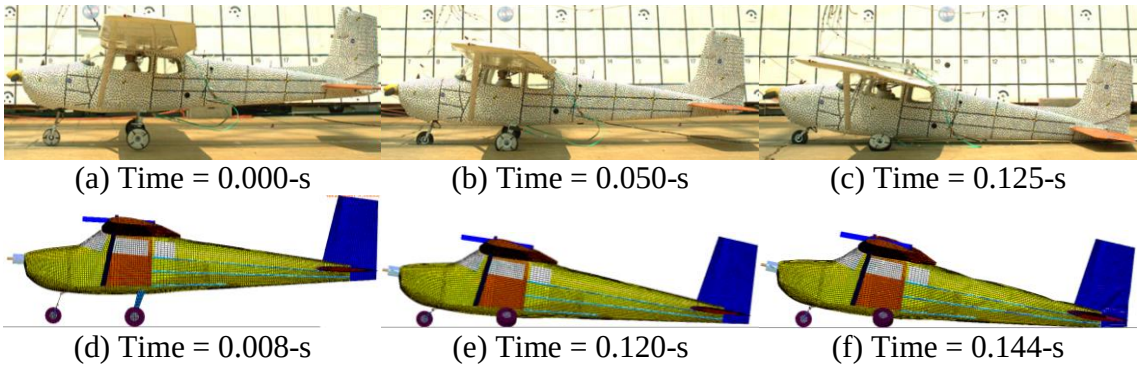

(a) Time = 0.000-s (b) Time = 0.050-s (c) Time = 0.125-s

(d) Time = 0.008-s (e) Time = 0.120-s (f) Time = 0.144-s

Figure 30. Time Sequence of Test 1 and ABAQUS analysis deformation.

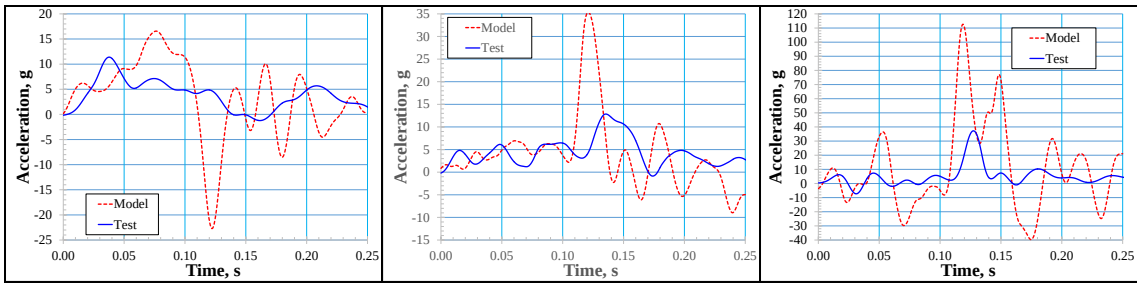

(a) Engine (b) DAS Box (c) Rear Bulkhead

Figure 31. Test 1 ABAQUS/Test Accelerations at Engine, DAS Box, and Rear Bulkhead

ABAQUS Test 2 Simulation

The ABAQUS model representing the Test 2 configuration is identical to the Test 1 configuration with the following exceptions. First, the number and position of the ELTs (five instead of four) is different. Second, the nose landing gear shock is replaced with a 1 in. long rigid beam to represent the damaged shock. The Test 2 configuration is heavier than Test 1, and two point masses (totaling 144-lb) were added to the model to match the weight and CG (within 0.25-in) of the test article. The impact surface in Test 2 is soil (30-in. deep), which is modeled in ABAQUS with 38,400 eight-node brick elements measuring 4 in. long by 3 in. wide by 2.5 in. deep. Soil properties are represented with the Mohr-Coulomb plasticity model with a density of 1.86e-4 lbf-s^2/in.

and a friction angle of 25-degrees. The model required 56 hours of wall clock time on an 8-processor Windows 7 workstation using ABAQUS/Explicit version 6.12 to simulate 0.25-seconds of impact, which is noticeably higher than the Test 1 runtime due to the additional soil elements and contact with the soil. Nodal acceleration time histories at accelerometer locations were extracted from the results file.

A sequence of photographs taken from the high-speed camera is shown in Figure 32, along with corresponding views of the model deformation. The collapse of the nose wheel and crushing of the bottom engine cowling is evident. In general, the model captures the kinematics of the fuselage impact with the soil accurately but does not capture the buckling of the fuselage or the fracture of the port wing. During the test, the nose gear separated from the firewall while the wheel was completely buried in the soil, and the exact time of separation is unknown. In the simulation, the connector elements on the nose gear are designed to break at a bending moment of 200,000 lbf-in (corresponding to time 0.05-seconds after nose impact).

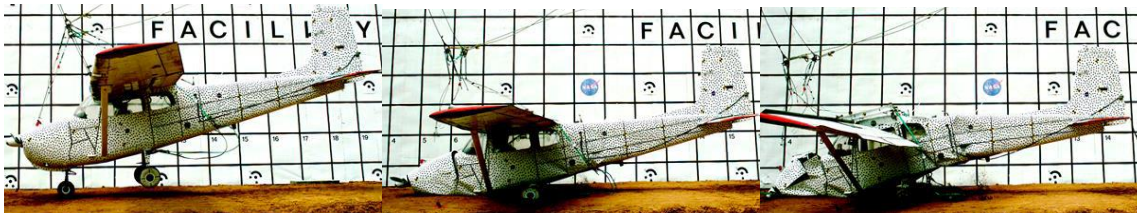

(a) Time = 0.000-s (b) Time = 0.111-s (c) Time = 0.169-s

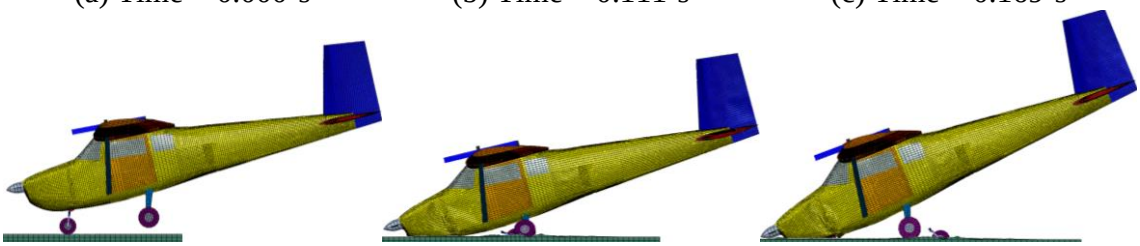

(d) Time = 0.000-s (e) Time = 0.111-s (f) Time = 0.169-s

Figure 32. Time Sequence of Test 2 and ABAQUS Analysis Deformation

A fringe plot of the predicted vertical displacement of the soil is shown in Figure 33(a), compared with a post-test photograph showing the soil deformation pattern in Figure 33(b). The model matches the overall shape of the deformation pattern. The main gear furrows were 96-inches long, and the analysis predicted 92-inches. Similarly, the nose gear furrow was 38-inches long and the analysis predicted 44-inches. The predicted location of maximum soil displacement matches the test data, as well; however, the maximum displacement of the model (9.60-inches.) is lower than the measured maximum of 11-inches. This finding is an indication that the soil model may be too stiff.

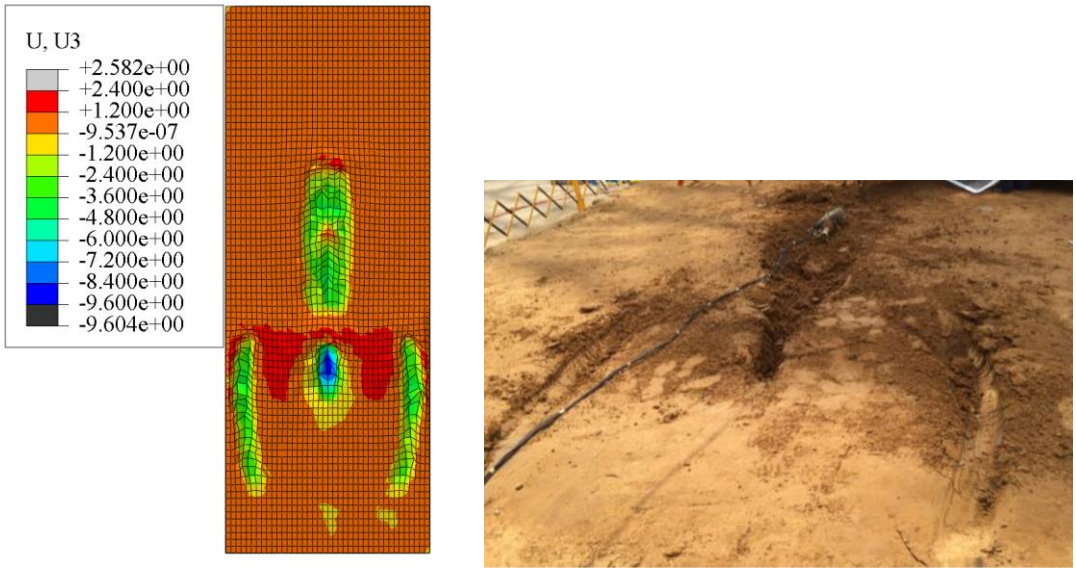

(a) Fringe plot of soil vertical deformation (b) Post-test photograph of soil

Figure 33. Test 2 ABAQUS/Test Soil Deformation

Time history comparisons of vertical accelerations are plotted at three locations (the engine, the DAS box, and the rear bulkhead) in Figure 34. The responses at the engine and rear bulkhead again reveal high oscillations in the model. Differences in the predicted and actual accelerations at the engine and bulkhead can be attributed to many factors including incorrect soil properties, premature breakage of the nose gear in the simulation, and failure to predict buckling of the aft fuselage. Predicted responses for

the DAS box exhibit more oscillations than seen in the test data; however the average and maximum acceleration is approximately the same as the test.

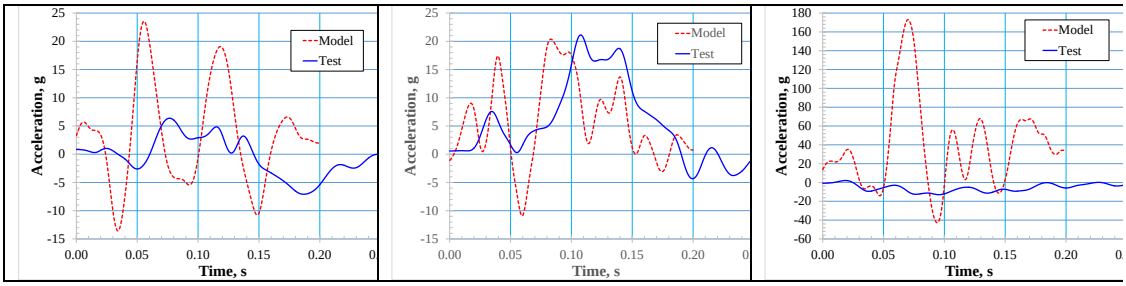

(a) Engine (b) DAS Box (c) Rear Bulkhead

Figure 34. Test 2 ABAQUS/Test Accelerations at Engine, DAS Box, and Rear Bulkhead

ABAQUS Test 3 Simulation

The ABAQUS model representing the Test 3 configuration is shown in Figure 35. A nominal shell element edge length of 1.5-in. was used. This model contains 98,177 nodes, 191 beam elements, 72,827 shell elements, 848 solid elements, 37 multi-point constraints, 8 materials, 4 revolute connectors (wheel axles), and 19 concentrated masses. Four point masses (totaling 110 lbs) were added to the model to match the weight and CG (within 0.25 in) of the test article. Major components (wing, fuselage, empennage, landing gear, etc.) are represented with the same types of elements as described for Test 1 and Test 2. The impact surface in Test 3 is soil (30 in. deep), which is modeled in ABAQUS with 63,360 eight-node brick elements measuring 4-inch long by 3-inch wide by 2.5-inch deep and uses the same properties as given for Test 2. Preliminary simulations and model validation are being performed and will be presented in a future paper.

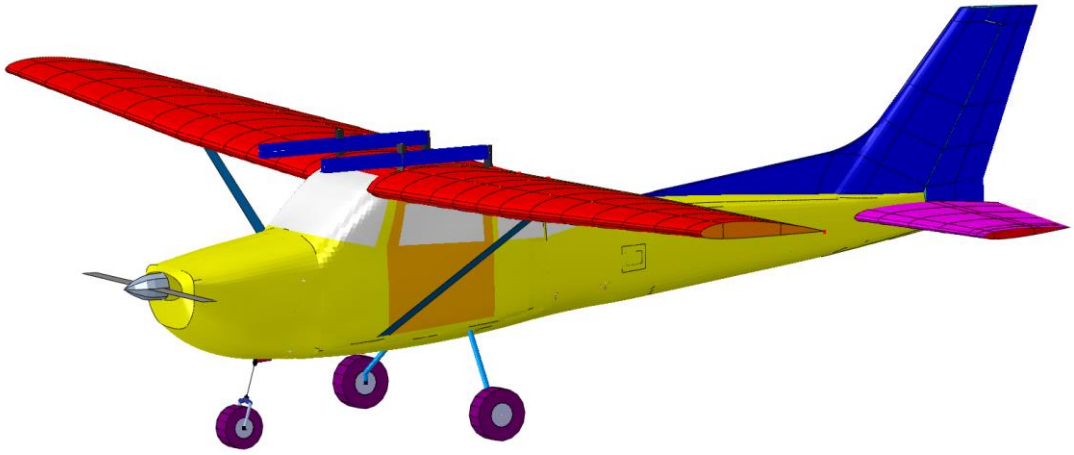

Figure 35. Test 3 ABAQUS Model

CONCLUSION

Three Cessna 172 crash tests were conducted at NASA's Landing and Impact Research Facility (LandIR) in the summer of 2015. The crash tests provided a baseline set of data to evaluate the crash loads and reliability of Emergency Locator Transmitters (ELT) under various crash attitudes and terrains. Test 1 was conducted on a hard surface, while Test 2 and Test 3 were on soil. Only minor damage was seen for the airplane used in Test 1. The main gear leaf springs absorbed the vertical impact velocity without showing signs of permanent damage. The belly of the aircraft was undamaged during the test.

Tests 2 and 3, while different in their impact attitudes, both resulted in the airplane flipping over and sustaining damage on the nose and tail. These similar results are due to the nose gear contacting and penetrating the dirt surface, causing a large rotation around the front of the airplane. Large amounts of damage were evident in the nose gear, engine firewall area and tail. Despite Test 3 having a tail strike configuration, causing a pitch-down rotation effect, the nose gear still penetrated the soil, and the aircraft flipped over about the nose. The tail was nearly detached from the rest of the structure, and significant damage was seen in the engine firewall area.

The analysis results for both LS-DYNA and ABAQUS highlight the different considerations that must be made to calibrate and validate full-scale crash models. Because Test 1 was a hard landing and the loads were generally in the lower elastic range, the model agreement was reasonable. With contact on a rigid surface, friction was the only parameter that was calibrated.

For Test 2, the presence of soil introduced a much different kinematic response and severe loading, causing permanent deformation. The simulation responses were highly sensitive to soil density and moisture content, which affect both soil bulk stiffness and yield strength. The amount of compaction influences the soil density and the moisture content influences the stiffness of the soil, as well as the coefficient of friction between the soil and an impacting surface. In the Test 2 models, the soil was represented using Lagrangian solid elements, which can distort severely under compaction and shearing. Model stability is dependent on the soil mesh. Even though soil calibration testing was performed, it can be difficult to translate the data obtained into a soil material model and to account for soil variability.

At the first instance of impact, the nose and main landing gear had to be modeled correctly. The nonlinear force/deflection curves for the nose strut were assumed based on heritage, but testing will be performed to verify those properties. The main landing gear was composed of steel, and the yield stress of those steel parts have to be verified. If the yield stress is too high, the kinematics of the airframe will not match.

For the airframe, the buckling and crippling of thin walled sections had to be represented accurately to predict the load distribution within the airframe. Considerations must be made for the level of fidelity in the shell mesh and how much detail was necessary to account for stringers, stiffeners, and discontinuities such as

holes and frame interfaces. The model is an approximation based on coarse laser scan and available reverse engineering software. The aluminum properties are assumed, and the actual strength properties may differ significantly due to aging. Coupon testing from the test articles will be conducted to determine the aluminum yield properties.

The tests provided a highly valuable set of data on severe but survivable crashes. Results from the validated models of Tests 1-3 will be used to establish the range of expected loads and responses for ELTs for updated requirements. Future publications will provide model calibration and validation results. Parameters that will be calibrated include landing gear stiffness, soil stiffness and strength, and airframe stiffness and strength. Validation of the models will require comparisons of kinematic response, progressive failure patterns, and acceleration time histories. The modeling guidelines and lessons learned for simulating full-scale crashes with both LS-DYNA and ABAQUS will be used for future test and analysis activities at LandIR.

ACKNOWLEDGEMENTS

This research was funded by Emergency Locator Transmitter Survivability and Reliability (ELTSAR) Project under the Search and Rescue (SAR) Program located at NASA Goddard Space Flight Center. Thanks to all SAR Program and ELTSAR management for their support and all of the engineers and technicians at the NASA LandIR facility for working with the utmost competence and efficiency to achieve three successful tests in such a short timeframe.

REFERENCES

1. NASA. "NASA's Gantry: Past, Present and Future Asset to Exploration." http://www.nasa.gov/centers/langley/news/factsheets/fs-2007-08-138-larc.html.
2. Jackson, K.E., Boitnott, R.L., Fasanella, E.L., Jones, L.E., and Lyle, K.H. "A History of Full-Scale Aircraft and Rotorcraft Crash Testing and Simulation at NASA Langley Research Center." NASA TM-2004-0191337. January 2004.

3. Hurley, T. R. and Vandenburg, J. M., editors, "Small Airplane Crashworthiness Design Guide," AGATE Report Reference No. AGATE-WP3.4-034043-036, Simula Technologies Reference No. TR-98099, April 2002.
4. Thomas, M., Chitty, D., Gildea, M., and T'Kindt, C, "Constitutive Soil Properties for Unwashed Sand and Kennedy Space Center," NASA/CR-2008-215334, July 2008.
5. Annett, M.S., et al. "Evaluation of the First Transport Rotorcraft Airframe Crash Testbed (TRACT 1) Full-Scale Crash Test." NASA TM-2014-218543. October 2014.
6. Society of Automotive Engineers, Recommended Practice: Instrumentation for Impact Test – Part 1, Electronic Instrumentation, SAE J211/1, March 1995.
7. Code of Federal Regulations - Title 14: Aeronautics and Space, Part 23: Airworthiness Standards: Normal, Utility, Acrobatic, and Commuter Category Airplanes, 23.562 - Emergency landing dynamic conditions.
8. LS-DYNA Keyword User's Manual, Version 971, Livermore Software Technology Company, Livermore, CA, August 2006.
9. ABAQUS, ABAQUS User's Manual, Vol III, Version 6.12, Dassault Systèmes Simulia Corp., Pawtucket, RI, 2012.
10. Mukhopadhyay, V., Hsu, S., Mason, B.H., Sleight, D.W., Jones, W.T., Chu, J., Hicks, M.D., Spangler, J.L., Kamhawi, H., and Dahl, J. L., "Adaptive Modeling, Engineering Analysis and Design of Advanced Aerospace Vehicles," AIAA Paper 2006-2182, 47th AIAA/ASME/ASCE/AHS/ASC SDM Conference, Newport, Rhode Island, May 1-4, 2006.